Nanoscale

Accepted Manuscript

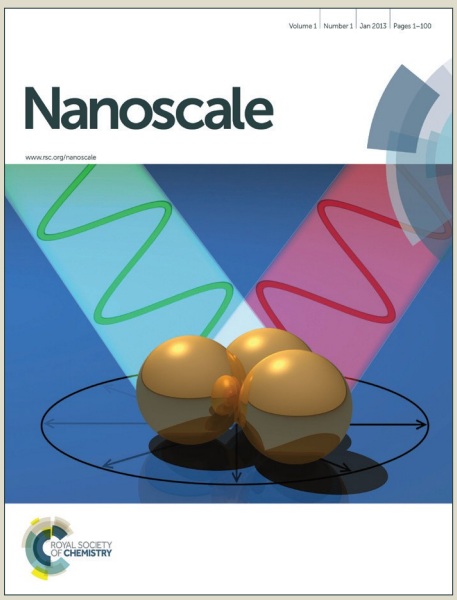

ROYAL SOCIETY OF CHEMISTRY

www.rsc.org/nanoscale

Nanoscale

PAPER

Electronic and geometric structures of Au_{30} clusters: A network of 2e-superatom Au cores protected by tridentate protecting motifs with u_3-S†

Received 00th January 20xx,
Accepted 00th January 20xx

DOI: 10.1039/x0xx00000x

www.rsc.org/

Zhimei Tian [a,b] and Longjiu Cheng*[a]

Density functional theory calculations have been performed to study the experimentally synthesized $Au_{30}S(SR)_{18}$ and two related $Au_{30}(SR)_{18}$ and $Au_{30}S_2(SR)_{18}$ clusters. The patterns of thiolate ligands on the gold cores for the three thiolate-protected Au_{30} nanoclusters are on the basis of the "divide and protect" concept. A novel extended protecting motif with u_3-S, $S(Au_2(SR)_2)_2AuSR$, is discovered, which is termed as tridentate protecting motif. The Au cores of $Au_{30}S(SR)_{18}$, $Au_{30}(SR)_{18}$ and $Au_{30}S_2(SR)_{18}$ clusters are Au_{17}, Au_{20} and Au_{14}, respectively. The superatom-network (SAN) model and superatom complex (SAC) model are used to explain the chemical bonding patterns, which are verified by chemical bonding analysis based on the adaptive natural density partitioning (AdNDP) method and aromatic analysis on the basis of nucleus-independent chemical shifts (NICS) method. The Au_{17} core of $Au_{30}S(SR)_{18}$ cluster can be viewed as a SAN of one Au_6 superatom and four Au_4 superatoms. The shape of the Au_6 core is identical to that revealed in the recently synthesized $Au_{18}(SR)_{14}$ cluster. The Au_{20} core of $Au_{30}(SR)_{18}$ cluster can be viewed as a SAN of two Au_6 superatoms and four Au_4 superatoms. The Au_{14} core of $Au_{30}S_2(SR)_{18}$ can be regarded as a SAN of two pairs of two vertex-sharing Au_4 superatoms. Meanwhile, the Au_{14} core is a 8e-superatom with $1S^21P^6$ configuration. Our work may aid understanding and give new insights into chemical synthesis of thiolate-protected Au clusters.

1. Introduction

Thiolate-protected gold nanoclusters ($Au_m(SR)_n$) have been widely studied due to their interesting optical, electronic and charging properties, as well as potential applications in catalysis, biomedicine and nanoelectronics.[1-5] The first breakthrough of the $Au_m(SR)_n$ nanoclusters crystallization is the crystal determination of $Au_{102}(SR)_{44}$ reported by Kornberg group.[1] $Au_{25}(SR)_{18}^-$ cluster is another breakthrough, and the crystal structure of which is reported separately by two groups.[6, 7] Subsequently, $Au_{38}(SR)_{24}$,[8] $Au_{36}(SR)_{24}$,[9-11] $Au_{28}(SR)_{20}$,[12] $Au_{23}(SR)_{16}^-$,[13] $Au_{24}(SR)_{20}$,[14] $Au_{20}(SR)_{16}$, $Au_{18}(SR)_{14}$,[15, 16] $Au_{133}(SR)_{52}$,[17, 18] and $Au_{130}(SR)_{50}$,[19] crystal structures are determined. Theoretical predictions of $Au_{25}(SR)_{18}$,[20-22] $Au_{38}(SR)_{24}$,[23-28] and $Au_{130}(SR)_{50}$,[29] clusters have been reported by several groups and confirmed by experiments.

In 2013, Dass et al. reported the synthesis and separation of the green $Au_{30}(SR)_{18}$ cluster and got the formula.[30] Later, this group[31] synthesized the $Au_{30}S(SR)_{18}$ cluster and concluded that $Au_{30}(SR)_{18}$ cluster was converted to $Au_{30}S(SR)_{18}$ cluster during the crystallization. Zheng et al.[32] also crystallized the $Au_{30}S(SR)_{18}$ cluster independently. The two works reveal the cluster with a novel u_3-S bridging and thiolate co-protecting layer, which is the first report of u_3-S bridging in $Au_m(SR)_n$ nanoclusters. The u_3-S bonding was suggested in the non-staple unit Au_{41}(S-Eind)$_{12}$ (Eind-SH is 1,1,3,3,5,5,7,7-octaethyl-s-hydrindacene-4-thiol) cluster,[33] and the u_3-S surface motif has been observed in $Au_3Ag(\mu_3\text{-}O)(PPh_2py)_3^{2+}$ cluster before.[34] Such a u_3-S bonding is theoretically predicted in $Au_mS_n^-$ and $(Au_2S)_n$ clusters.[35-37]

The appropriate aufbau rule of super shells for spherical Au clusters is $|1S^2|1P^6|1D^{10}|2S^21F^{14}|2P^61G^{18}|\ldots$ (S–P–D–F–G–H– denote angular-momentum characters), associated with magic numbers 2, 8, 18, 34, 58, …. Häkkinen et al. proposed the superatom complex (SAC) model.[2] According to the model, one determines the valence-electron count (V) of $Au_m(SR)_n^q$ cluster (where q is the charge of the cluster) by $V = m - n - q$. Each gold contributes one valence electron and each SR localizes one electron; if there is S in cluster, each S localizes two electrons. The model provides a useful perspective to explain why certain compositions are stable. The SAC model has been successfully used to interpret the stability of $Au_m(SR)_n$ nanoclusters with spherical shells and magic numbers.[6, 38-40]

According to SAC model,[2] $Au_{30}S(SR)_{18}$ cluster is a 10e-compound. Cheng and Yang[41] proposed the superatom-network (SAN) model to explain the electronic stability of non-spherical shells of metal clusters. The electronic stability of the 4e thiolate-protected nanoparticles $Au_{18}(SR)_{14}$, $Au_{20}(SR)_{16}$ and $Au_{24}(SR)_{20}$ follows the SAN model and the Au_8 cores of the three clusters should be viewed as two non-conjugate 4-center 2-electron (4c-2e) tetrahedral Au_4 superatoms.[41] The Au_9^{5+} core in experimentally determined

*Email: clj@ustc.edu.
[a]Department of Chemistry, Anhui University, Hefei, Anhui, 230601, China.
[b]School of Chemistry and Materials Engineering, Fuyang Teachers College, Fuyang, Anhui, 236037, China.

†Electronic Supplementary Information (ESI) available: The AdNDP localized natural bonding orbitals of the valence shells of $Au_{30}S(SH)_{18}$ cluster. IR spectra, absorption spectra and coordinates of $Au_{30}S(SCH_3)_{18}$, $Au_{30}(SCH_3)_{18}$ and $Au_{30}S_2(SCH_3)_{18}$ clusters. See DOI: 10.1039/x0xx00000x

$Au_{18}(SR)_{14}$ cluster can be viewed as a unique combination of two fused octahedral Au_6 superatom units according to the SAN model.[15]

The "divide-and-protect" approach was originally proposed by Häkkinen et al.,[23] that is, a $Au_m(SR)_n$ cluster can be viewed as an Au core fully covered by various staple motifs (with known structures but different lengths). Staple motifs like $Au_x(SR)_{x+1}$ units are commonly observed in the surface protected layers of $Au_m(SR)_n$ nanoclusters. Maksymovych et al. studied adsorption of methylthiolate on Au(111) and found Au adatom-induced self-assembly via formation of a linear monomer bonding motif.[42] Jadzinsky et al. found monomer and extended dimer units in $Au_{102}(SR)_{44}$, which they termed the "staple" motif.[1] The dimer staple motif is also observed in the experimentally synthesized $Au_{25}(SR)_{18}^-$, $Au_{38}(SR)_{24}$, $Au_{28}(SR)_{20}$ and $Au_{36}(SR)_{24}$ clusters.[6, 8, 11, 12] The trimer staple motif is revealed in $Au_{28}(SR)_{20}$ and $Au_{23}(SR)_{16}^-$ clusters.[11, 13, 43] The dimer and trimer motifs were predicted in small thiolated gold clusters.[44] Tetramer motif has been theoretically determined to be part of the thiolated Au_{15} cluster,[45] and then is revealed in the synthesized $Au_{24}(SR)_{20}$ and $Au_{18}(SR)_{14}$ clusters.[14-16] The gold-thiolate rings such as $Au_8(SR)_8$ and $Au_6(SR)_6$ rings have been revealed in $Au_{20}(SR)_{16}$ and $Au_{22}(SR)_{18}$ clusters, respectively.[46, 47] The bridging -SR ligand was first predicted from DFT calculations in $Au_{13}(SR)_n$ (n = 4, 6, 8) clusters,[48] and later revealed experimentally in $Au_{23}(SR)_{16}^-$ cluster.[13]

The "divide and protect" scheme has been widely used to predict $Au_m(SR)_n$ clusters,[7, 27, 49-51] which can be viewed as Au cores protected by protecting motifs. However, the size of the Au cores and the length of the protecting motifs are uncertain since the Au-Au distances in Au cores and those between Au cores and Au protecting motifs are similar. The recently synthesized $Au_{30}S(SR)_{18}$ is an interesting cluster with u_3-S unit,[31, 32] and the u_3-S unit is viewed as a protecting motif. However, based on the "divide and protect" scheme and SAN model, we think that the u_3-S should not be regarded as an actual ligand; rather it is $S(Au_2(SR)_2)_2AuSR$ that constitutes the protective unit. Herein the $S(Au_2(SR)_2)_2AuSR$ is termed as tridentate protecting motif, which is a new type of extended protecting motif with three branches. This work tries to give a new perspective of the Au_{30} cluster from its geometric and electronic structure based on "divide and protect" scheme and SAN model. The tridentate protecting motif enriches the family of motifs. We envision $Au_{30}S_2(SCH_3)_{18}$ cluster formed by addition of a second u_3-S to $Au_{30}S(SCH_3)_{18}$ cluster (methylthiolate is chosen for convenience). Considering $Au_{30}(SCH_3)_{18}$ cluster is in C_2 symmetry, if we add a second u_3-S to it symmetrically, what structure will the cluster keep? On the other hand, the synthesis of body-centered cubic $Au_{38}S_2(SR)_{20}$ nanocluster with two u_3-S has been reported recently.[52] Thus, it is natural for us to create $Au_{30}S_2(SCH_3)_{18}$ cluster.

2. Computational methods

2.1 Structure determination

Starting from the experimental crystal structure of $Au_{30}S(StBu)_{18}$,[31] density functional theory (DFT) calculations have been carried out. Due to computational difficulty, we replace R group with CH_3 in our calculations. The TPSS (Tao, Perdew, Staroverov, and Scuseria)[53] functional is used in DFT calculations, which has been proven reliable in prediction of $Au_m(SR)_n$ nanoclusters,[38, 54-56] with LanL2dz basis set used for Au which accounts for the relativistic effective core potentials, and 6-31G* basis set used for S, C and H atoms. Harmonic vibrational frequency analyses are carried out at the same level to confirm that the structures are true minima. The quality of self-consistent field (SCF) convergence tolerance is set with a convergence criterion of 1×10^{-5} hartree on total energy and electron density, 2×10^{-3} hartree/Å on the gradient, and 5×10^{-3} Å on the displacement in our calculations. Symmetry type of the Au_{30} clusters is given at 0.01 Å tolerance. The calculations of molecular orbital (MO) and the natural bond orbital (NBO)[57] analyses are also calculated at the same level. All calculations are carried out using the Gaussian 09 package.[58] Molecular visualization is performed using MOLEKEL 5.4.[59]

2.2 Adaptive natural density partitioning (AdNDP) method

Chemical bonding analysis is performed using the adaptive natural density partitioning (AdNDP) method developed by Zubarev and Boldyrev.[60, 61] This method is widely used to analyse the chemical bondings in boron clusters,[60, 62, 63] Au clusters[64, 65] and $Au_m(SR)_n$ nanoclusters.[5, 66] The algorithm is a generalization of the natural bonding orbital analysis and is based on diagonalization of the blocks of the first-order density matrix on the basis of natural atomic orbitals. AdNDP analysis is dependent on the choice of the threshold values for the occupation numbers which is inherited from the parental NBO analysis. This method accepts only those bonding elements whose occupation numbers (ON) exceed the specified threshold values, which are usually chosen to be close to 2.00 |e|. AdNDP is based on the concept of the electron pair as the main element of chemical bonding models, which recovers both Lewis bonding elements (1c-2e and 2c-2e objects) and delocalized bonding elements (nc-2e) with n ranging from one to the total number of atoms in the whole molecule.

2.3 Nucleus-independent chemical shifts (NICS) method

Aromaticity is one of the most important concepts in chemistry, which can be applied not only to planar two-dimensional molecules but also to diverse structures of three-dimensional molecules.[67] In 1996, nucleus-independent chemical shifts (NICS) method was proposed as an aromaticity/antiaromaticity criterion by Schleyer et al,[68] which uses the absolute magnetic shieldings as a magnetic index of aromaticity. NICS value is the most widely used quantitative measure for aromaticity. Negative NICS values mean aromaticity, whereas positive NICS values mean antiaromaticity. NICS is an effective aromaticity criterion, which has been successfully used to predict the aromaticity of aromatic hydrocardons,[68] boron clusters, fullerenes,[67] and all-metal compounds,[69] etc.

NICS values in this work are calculated with TPSS/Lanl2dz and 6-31G* method through the gauge-including atomic orbital (GIAO) method[70] implemented in Gaussian 09. NICS uses a ghost atom (termed ''bq'' after the ghost Banquo in Shakespeare's Macbeth), namely, one with no proton, neutron or electron, which is placed at any desired location.[71] This ghost atom is nothing but a sensor for the magnetic environment at the point. The ghost atom senses the magnetic environment and reports the chemical shielding (absolute chemical shift) through the use of GIAO. The NICS value is taken to be the negative of the calculated shielding.

3.Results and discussion

Based on the crystal structure $Au_{30}S(StBu)_{18}$, we obtained the original structure of $Au_{30}S(SCH_3)_{18}$. Then, the original structures of $Au_{30}(SCH_3)_{18}$ and $Au_{30}S_2(SCH_3)_{18}$ clusters are obtained by removing the u_3-bridging S

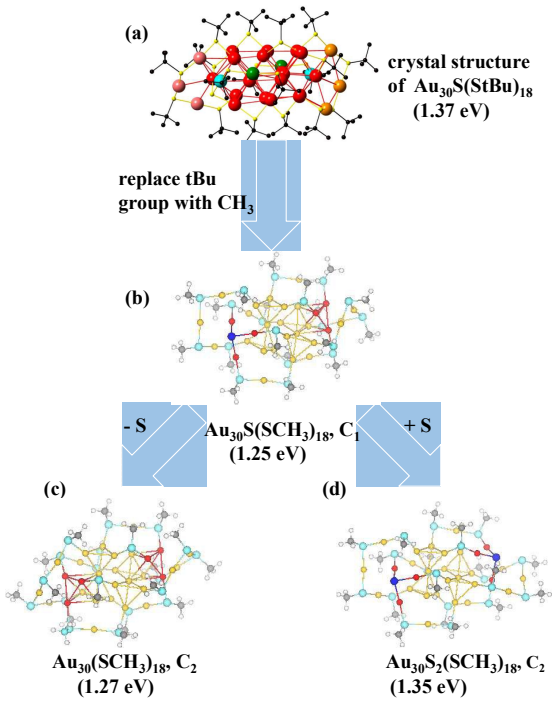

Fig. 1 (a) Single crystal XRD structure of $Au_{30}S(StBu)_{18}$ from ref 31, (b) the optimized structure of $Au_{30}S(SCH_3)_{18}$ cluster, (c) the optimized structure of $Au_{30}(SCH_3)_{18}$ cluster, (d) the optimized structure of $Au_{30}S_2(SCH_3)_{18}$ cluster. The clusters are obtained at the TPSS/LanL2dz (Au) and 6-31G* (S, C, H) level of theory. Au, red and yellow; S, baby blue and blue (u_3-S); C, gray; H, white. Enclosed are HOMO-LUMO gaps of the clusters.

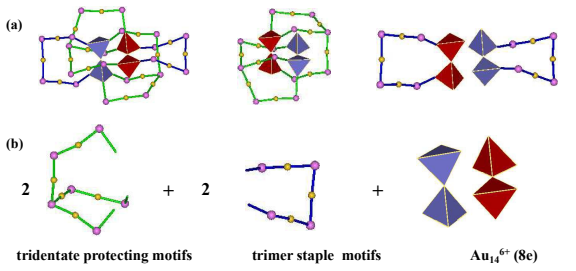

Fig. 2 (a) Structure model of $Au_{30}S_2(SR)_{18}$. R groups are removed for clarity. The $S(Au_2(SR)_2)_2Au(SR)$ and $Au_3(SR)_4$ oligomers are given as ball-and-stick models (Au: yellow; S: pink), in which the sticks are shown in different colors by their groups. The Au cores are shown as polyhedra. (b) Model of Au_{14}^{6+} core plus tridentate protecting motifs and trimer staple motifs.

and adding a second u_3-bridging S, respectively. Then we optimize the clusters using TPSS functional. The structures of them are given in Fig. 1.

3.1 Structures

From Fig. 1, we can see that the geometric structures of the three Au_{30} clusters are very novel. The HOMO-LUMO gap of $Au_{30}S(SCH_3)_{18}$ cluster is 1.25 eV, which is smaller than that of $Au_{30}S(StBu)_{18}$ cluster (1.37 eV, Fig. 1a) computed by PBE functional.[31] Dass et al. reported that the cluster features an Au_{20} core protected by a layer, that is, a combination of monomeric and trimeric gold-thiolate units, bridging thiolates, and a single u_3-sulfur. Zheng et al. reported that the cluster consists of an Au_{22} core capped by a mixed layer of staple Au-thiolate units, bridging thiolates and a μ_3-S. In contrast, our results (Fig. 1b) reveal that the cluster is composed of an Au_{17} core protected by a combination of a new tridentate protecting motif $S(Au_2(SR)_2)_2AuSR$ with a μ_3-S, two monomeric, two trimeric units and one bridging -SR on the basis of the "divide and protect" concept.[23] Interestingly, the tridentate protecting motif has three branches, one AuSR and two $Au_2(SR)_2$, which is distinctly different from common staple motifs. The branching motif as a union protects the Au_{17} core in $Au_{30}S(SR)_{18}$ cluster. In this work, the three Au atoms connected by u_3-S in Au_{20} and Au_{22} cores of previous reports are the compositions of the tridentate protecting motif. The tridentate protecting motif provides an alternative picture for the understanding of bonding in $Au_{30}S(SR)_{18}$ cluster. $Au_{30}(SCH_3)_{18}$ cluster is in C_2 symmetry and it is a 12e-compound with a HOMO-LUMO gap of 1.27 eV. According to the "divide and protect" scheme, $Au_{30}(SR)_{18}$ is viewed as $Au_{20}(Au_3(SR)_4)_2(SR)_2(Au(SR)_2)_4$. It is composed of one Au_{20} core protected by two bridging SR, two $Au_3(SR)_4$ and four $Au(SR)_2$. Note that the vertex-sharing Au_7 unit of the Au_{20} core is remarkably similar to the core of $Au_{28}(SR)_{20}$ cluster,[12, 43] which has been pointed out earlier.[31, 32]

From the analysis above, adding a u_3-S to $Au_{30}(SCH_3)_{18}$, the cluster changes to $Au_{30}S(SCH_3)_{18}$, meanwhile, the Au_{20} core changes to Au_{17} core. As shown in Fig. 1, $Au_{30}S_2(SCH_3)_{18}$ cluster is in C_2 symmetry, and it can be described as $Au_{14}(Au_3(SCH_3)_4)_2[S(Au_2(SCH_3)_2)_2AuSCH_3]_2$ based on "divide-and-protect" notation.[23] The Au_{14} core resembles the core in $Au_{28}(SR)_{20}$ cluster.[43] As the addition of a second u_3-S to $Au_{30}S(SCH_3)_{18}$, the Au cores change from Au_{17} to Au_{14}, indicating the Au cores become smaller. $Au_{30}S_2(SCH_3)_{18}$ is stable with a HOMO-LUMO gap of 1.35 eV. We have also optimized $Au_{30}S_2(SR)_{18}$ cluster with real ligand R=t-Bu. The results show that the cluster is stable with a HOMO-LUMO gap of 1.41 eV, and harmonic vibrational frequency analyses confirm that the structure is a true minimum. Although the $Au_{30}S_2(SCH_3)_{18}$ cluster has not been synthesized yet, it may be synthesized in future. The structural model of $Au_{30}S_2(SR)_{18}$ is shown in Fig. 2. Remarkably, two tridentate protecting motifs are discovered, and the three terminal S legs of each $S(Au_2(SR)_2)_2Au(SR)$ anchor to three Au atoms of the farther vertex-sharing Au_7 kernel (Fig. 2a). The tridentate protecting motif adopts a branching conformation, with average SR-Au-SR angle of 172.7° and Au−SR−Au angle of 93.3°. The tridentate protecting motif interacts with the neighbouring vertex-sharing Au_7 kernel exclusively through Au_{motif}–Au_{kernel} bonding. The average Au···Au distance of 3.11 Å indicates strong aurophilicity interaction between the motif and the neighbouring Au_7 kernel. Thus, the interaction modes between the tridentate protecting motifs and the Au_{14} kernel include both the "clamping" mode which has S-Au kernel bonding between the motif and Au kernel, and the aurophilicity interactions. The two terminal S legs of the trimer staple motifs clamp to two Au atoms of the nearby Au_7 kernel. By anchoring and clamping of the protecting motifs, the cluster can keep stable. In this work, the "divide-and-protect" concept can be extended to tridentate protecting motif.

3.1 Chemical bonding analysis

To verify the structural prediction of the three Au_{30} clusters, the chemical bonding analysis is performed. Though there are ligand effects[72-74] on Au_{30} clusters when different ligands are used, here, we focus on the chemical bonding analysis. It is found that the structures do not change much when the $-SCH_3$ group is replaced by -SH group, and the chemical bonding pattern of the Au cores do not change. Thus, we use -SH instead of $-SCH_3$ for simplicity and clarity in chemical bonding analysis, and this method

has been used to study $Au_{38}(SR)_{24}$ and phosphine-protected Au_{20} clusters before.[5, 75]

The binding framework of the valence shells of $Au_{30}S(SH)_{18}$ cluster using AdNDP is in Fig. S1, ESI†. According to the AdNDP analysis, there are 19 lone pairs (LP) on the 19 S atoms, 18 × 2c-2e localized S-H bonds with ONs = 1.98-1.99 |e| and 39 × 2c-2e localized Au-S bonds with ONs = 1.82-1.95 |e|. The cluster follows the SAN (5 × 2e) model in electronic structure. AdNDP analysis (Fig. 3a) reveals one 6c-2e bond with ON = 1.77 |e| and four 4c-2e bonds with ONs = 1.62-1.65 |e|. This 4c-2e binding pattern is in accordance with the experimentally synthesized 4e compounds $Au_{20}(SR)_{16}$, $Au_{24}(SR)_{20}$ and $Au_{24}(SeR)_{20}$ clusters.[3, 14, 46, 76] The Au_6 superatom exists in the recently experimentally produced $Au_{18}(SR)_{14}$ cluster.[15, 16] To display the chemical bonding more clearly, we only analyse the Au_{17} core of $Au_{30}S(SH)_{18}$ cluster while keeping its geometric structure. The results of AdNDP analysis are shown in Fig. 3b. The Au_{17} core is a 5 × 2e SAN, which consists of one Au_6 superatom and four Au_4 superatoms. The ON in the 6c-2e bond is 1.90 |e|, while the four 4c-2e bonds with ONs = 1.64-1.74 |e|.

$Au_{30}(SH)_{18}$ cluster follows SAN model (6 × 2e) in electronic structure, which can be viewed as a network of two Au_6 superatoms and four Au_4 superatoms stapled by two SH, four $Au(SH)_2$ and two $Au_3(SH)_4$ units. Meanwhile, the four Au_4 superatoms are two vertex-sharing units which can be regarded as two Au_7 cores. Fig. 4a displays the AdNDP localized natural bonding orbitals of the cluster. AdNDP analysis reveals two 6c-2e bonds with ON = 1.80 |e|, and four 4c-2e bonds with ONs = 1.62-1.64 |e|. Then we take Au_{20} core out of the cluster and analyze the chemical bonding pattern. The results of the AdNDP are shown in Fig. 4b. As shown in the figure, Au_{20} core can be viewed as a network of two Au_6 and four Au_4 superatoms. The ONs of the two 6c-2e bonds are 1.86 |e| and those of the four 4c-2e bonds are 1.65-1.77 |e|. The vertex-sharing conformation of Au_4 superatoms has been revealed in experimentally produced $Au_{20}(SR)_{16}$ and $Au_{36}(SR)_{24}$ clusters.[46, 77]

$Au_{30}S_2(SH)_{18}$ cluster follows SAN model (4 × 2e) in electronic structure, and it consists of a network of two pairs of vertex-sharing Au_4 superatoms. AdNDP in Fig. 5a reveals four 4c-2e bonds in the cluster and the ONs = 1.64-1.66 |e|. In order to clearly get the chemical bonding pattern of the cluster, we analyze the Au_{14} core of the cluster separately, and the results are shown in Figs. 5b and 5c. The Au_{14} core follows the SAN model, and it can be

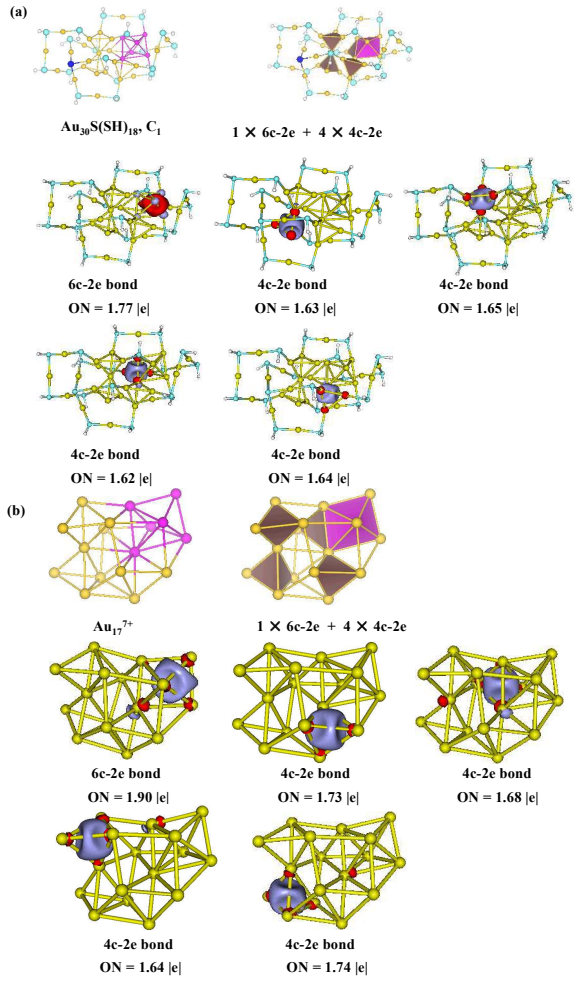

Fig. 3 (a) Structure, superatom-network model and AdNDP localized natural bonding orbitals of $Au_{30}S(SH)_{18}$. (b) Structure, superatom-network model and AdNDP localized natural bonding orbitals of Au_{17}^{7+} core of $Au_{30}S(SH)_{18}$ cluster. Au, yellow; S, baby blue and blue.

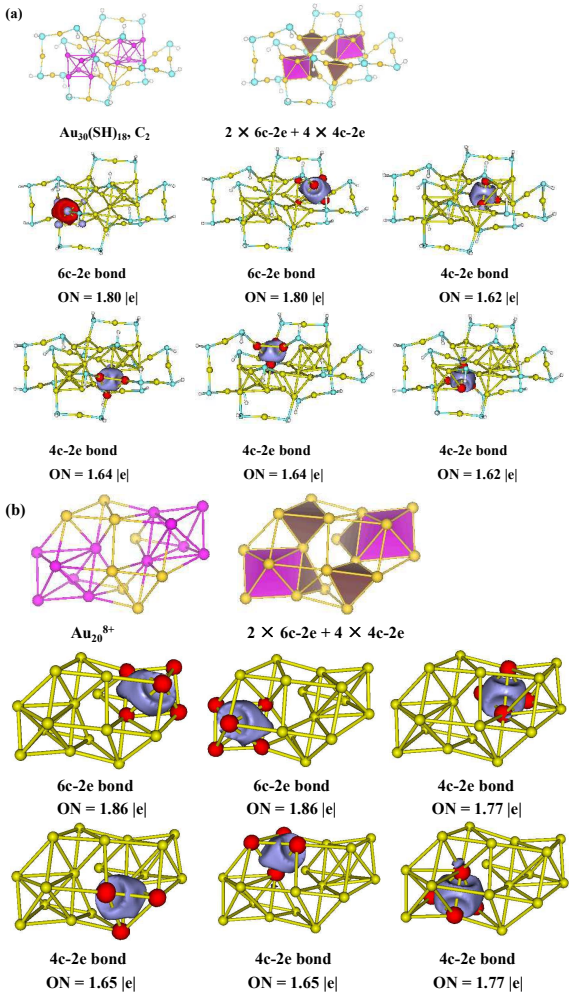

Fig. 4 (a) Structure, superatom-network model and AdNDP localized natural bonding orbitals of $Au_{30}(SH)_{18}$. (b) Structure, superatom-network model and AdNDP localized natural bonding orbitals of Au_{20}^{8+} core of $Au_{30}(SH)_{18}$ cluster. Au, yellow; S, baby blue.

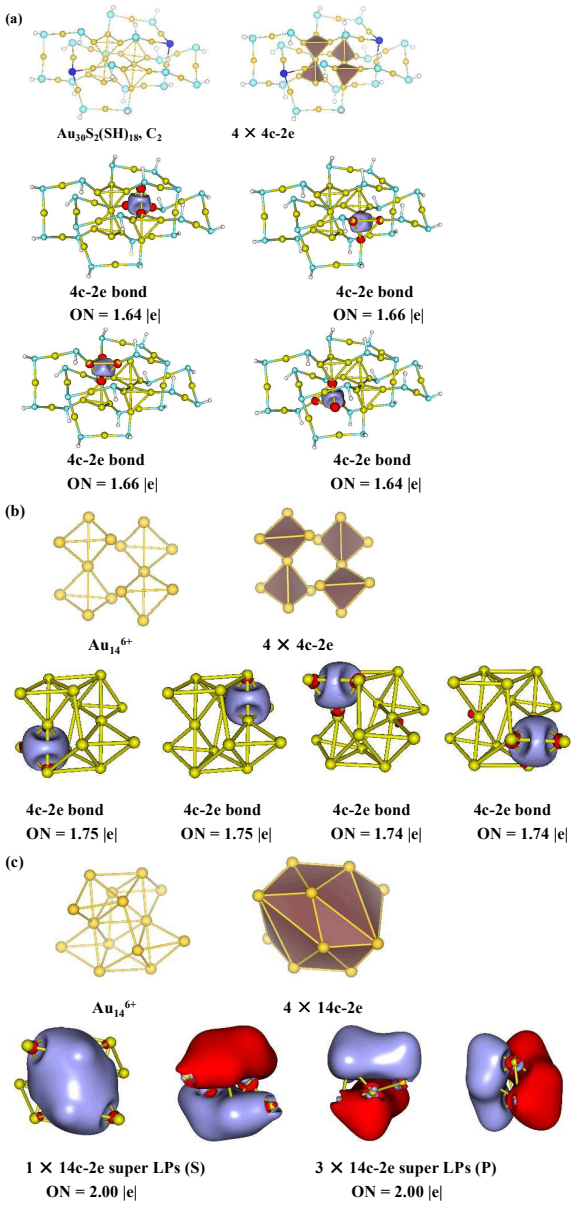

Fig. 5 (a) Structure, superatom-network model and AdNDP localized natural bonding orbitals of $Au_{30}S_2(SH)_{18}$. (b) Structure, superatom-network model and AdNDP localized natural bonding orbitals of Au_{14}^{6+} core of $Au_{30}S_2(SH)_{18}$ cluster. (c) Structure, superatom model and AdNDP localized natural bonding orbitals of Au_{14}^{6+} core of $Au_{30}S_2(SH)_{18}$ cluster. Au, yellow; S, baby blue and blue.

viewed as a network of four Au_4 superatoms (Fig. 5b). The four Au_4 superatoms are two vertex-sharing units which can be regarded as two Au_7 cores. AdNDP analysis reveals four 4c-2e bonds with ONs = 1.74-1.75 |e|. In Au_{14} core, the four 4c-2e bonds can delocalize in the whole range. The Au_{14} core has a valence electron count of 8, which follows the SAC model as well, with $1S^21P^6$ configuration of free electrons as expected from the counting rule.[2] AdNDP analysis reveals the fulfilled $1S^21P^6$ superatom orbitals in the core (Fig. 5c), which includes 1 × 14c-2e super 1S LP and 3 × 14c-2e super 1P LPs with ONs = 2.00 |e|. Moreover, similar to $Au_{28}(SR)_{20}$,[43] the superatomic

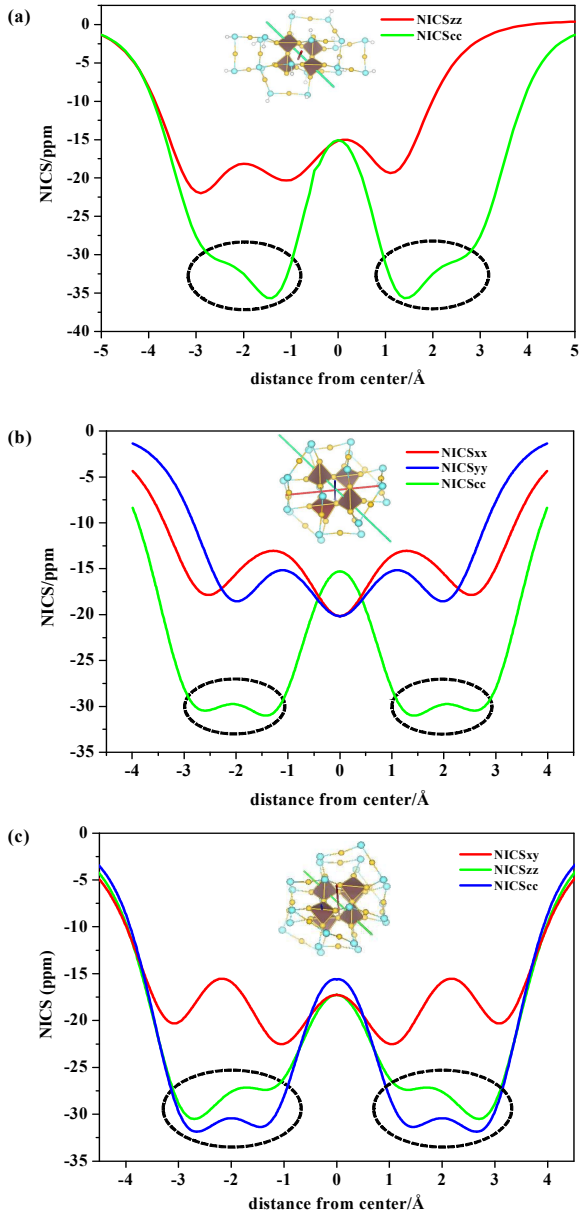

Fig. 6 (a) NICSzz- and NICScc-scan curves of $Au_{30}S_2(SH)_{18}$ cluster, (b) NICSxx-, NICSyy- and NICScc-scan curves of $Au_{28}(SR)_{20}$ cluster, (c) NICSxy-, NICSzz- and NICScc-scan curves of $Au_{36}(SR)_{24}$ cluster. NICSxx-, NICSyy- and NICSzz- are the scans along x, y and z axes, respectively; NICSxy-scan and NICScc-scan are the scans in xy-plane and along the centers of the Au_4 superatoms, respectively. The black dotted ovals in the figure signal the presence of Au_4 superatoms.

orbitals can also be found in the molecular orbitals of $Au_{30}S_2(SH)_{18}$ cluster (Fig. S3† in SI).

3.2 Aromaticity

To further confirm the structural prediction, NICS calculations are carried out. In 2001, Boldyrev and Wang et al. reported for the first time

experimental and theoretical evidence of aromaticity in Al_4^{2-}, an all-metal compound.[78] Rings with large negative NICS values are considered to be aromatic. The more negative the NICS values, the more aromatic the molecules are. The maximum negative value of NICS is found at the center of the Al_4^{2-} ring, and the NICS values at the centers are better suited for evaluation of the aromaticity for all-metal species.[79] σ-aromaticity is the aromaticity due to σ-electron delocalization first developed by Dewar[80] and later Exner and Schleyer.[81] The aromaticity of the Au_4 and Au_6 superatoms in $Au_{30}S(SH)_{18}$ and $Au_{30}(SH)_{18}$ clusters is σ-aromaticity due to $6d^1$ σ-electrons of Au atoms. The NICS values at the centers of Au_4 superatoms range from -32.2 to -29.6 ppm, whereas those of Au_6 superatoms vary from -17.1 to -16.6 ppm, indicating high aromaticity of the clusters. It is clearly that these values are much higher than that of the famous aromatic molecule C_6H_6 (-9.7 ppm). [68]

Stanger introduced the NICS-scan method,[82] which is analogous to the aromatic ring center shieldings approach. Here, we employ NICS-scan method to analyze the aromaticity of $Au_{30}S_2(SH)_{18}$ cluster. Fig. 6a displays the NICS-scan curves for $Au_{30}S_2(SH)_{18}$ cluster within the range of -5.0-5.0 Å. Note that NICS(0) position in the figure is the geometric center of the cluster. The green curve is obtained through scanning along two centres of the two non-conjugated Au_4 superatoms (coined as NICScc-scan) and the red curve is the scan along z-axis of the cluster (coined as NICSzz-scan). From the figure, we can see that the acromaticity along the centres of the two Au_4 superatoms is stronger than that along z-axis. The two black dotted ovals in the figure signal the presence of two independent Au_4 superatoms. In other words, the superatoms can be demonstrated existing by NICScc-scan method, which gives extra support to SAN model. NICS-scan method has been used to support SAN model in $Au_{20}(SR)_{16}$ cluster before.[41]

In order to verify the proposition that the superatoms can be proved existing through NICS-scan method, we take $Au_{28}(SR)_{20}$ and $Au_{36}(SR)_{24}$ clusters as two test cases. The Au_{14} core in $Au_{30}S_2(SH)_{18}$ cluster and that in $Au_{28}(SR)_{20}$ resemble each other. Based on the AdNDP analysis of Pei et al.[66], the Au_{14} and Au_{20} cores in $Au_{28}(SR)_{20}$ and $Au_{36}(SR)_{24}$ clusters can be viewed as networks of four and six Au_4 superatoms, respectively. The NICS-scan curves of $Au_{28}(SR)_{20}$ are plotted in Fig. 6b. The green curve scans along two centers of the two non-conjugated Au_4 superatoms, and NICS(0) position is set at the midpoint of the two centers of Au_4 superatoms. The aromatic properties along x-axis and y-axis within the range of -5.0-5.0 Å above the geometric center of the cluster are much weaker compared to NICScc-scan. Fig. 6c displays the NICS-scan curves of $Au_{36}(SR)_{24}$ cluster. NICS(0) position of NICSxy- and NICSzz-scan curves is the geometric center of the cluster, whereas that of the NICScc-scan curve is set at the mid-point of the two centers of the scanned Au_4. Coincidently, NICSzz-scan curve is also the scan along two independent Au_4 cores. From the figure, we can obtain that the two curves scanning along the centers of Au_4 superatoms (NICScc- and NICSzz-scan) signal the Au_4 superatoms, and the aromatic is more highly compared to NICSxy-scan. As shown in the figure displayed in dotted oval, the aromaticity brought by four Au_4 superatoms can be clearly seen. In a word, the Au_4 superatom can be proved existing based on NICS-scan method. The existence of the Au_4 cores is demonstrated from the aromaticity point of view.

4. Conclusions

Based on the "divide-and-protect" scheme, the electronic and geometric structures of the three related Au_{30} clusters have been investigated by first principle study. The Au cores of $Au_{30}S(SR)_{18}$, $Au_{30}(SR)_{18}$ and $Au_{30}S_2(SR)_{18}$ clusters are Au_{17}, Au_{20} and Au_{14}, respectively. This is supported both by chemical bonding analysis and aromatic analysis. The Au cores of the three clusters can de viewed as networks of 2e-superatoms. A unique tridentate protecting motif with u_3-S, $S(Au_2(SR)_2)_2AuSR$, is revealed in $Au_{30}S(SR)_{18}$ and $Au_{30}S_2(SR)_{18}$ clusters. The SAN and SAC models are used to characterize the bonding patterns of the three Au_{30} clusters. The Au_{17} core of $Au_{30}S(SH)_{18}$ cluster can be viewed as a superatom-network of Au_6 and Au_4 superatoms. The Au_6 superatom exists in the recently experimentally produced $Au_{18}(SR)_{14}$ cluster, and the Au_4 superatoms are present in experimentally synthesized $Au_{20}(SR)_{16}$, $Au_{24}(SR)_{20}$ and $Au_{24}(SeR)_{20}$ clusters. The Au_{20} core of $Au_{30}(SR)_{18}$ follows SAN model, and it can be viewed as a SAN of four Au_4 superatoms and two Au_6 superatoms. The Au_{14} core of $Au_{30}S_2(SR)_{18}$ cluster can be viewed as a SAN of four Au_4 superatoms. Meanwhile, the Au_{14} core is a 8e-superatom with $1S^21P^6$ configuration. $Au_{30}S_2(SR)_{18}$ cluster has two bitetrahedral Au_7 cores, and such a Au_7 kernel is associated with the experimentally determined structure of $Au_{20}(SR)_{16}$ cluster.

The NICS-scan method is used to analyze the aromaticity of $Au_{30}S_2(SR)_{18}$ cluster, and we find that the Au_4 superatoms can be clearly shown by NICS-scan curves which scan along two centers of Au_4 superatoms. In a word, the existence of superatoms in $Au_m(SR)_n$ nanoclusters can be demonstrated from analysis of both chemical bonding and aromatic perspectives. We believe that our work will give new insights into the electronic structures and stability of the three Au_{30} clusters. The concept of tridentate protecting motif can provide some references to the experimental synthesis of $Au_m(SR)_n$ clusters in future.

Acknowledgements

This work is supported by the National Natural Science Foundation of China (21273008, 21573001) and the Natural Science Foundation of Anhui Provincial University (2015KJ013). The calculations are carried out on the High-Performance Computing Centre of Anhui University.

References

1. P. D. Jadzinsky, G. Calero, C. J. Ackerson, D. A. Bushnell and R. D. Kornberg, *Science*, 2007, **318**, 430.
2. M. Walter, J. Akola, O. Lopez Acevedo, P. D. Jadzinsky, G. Calero, C. J. Ackerson, R. L. Whetten, H. Grönbeck and H. Häkkinen, *Proc. Natl. Acad. Sci.*, 2008, **105**, 9157.
3. M. Z. Zhu, H. F. Qian and R. C. Jin, *J. Am. Chem. Soc.*, 2009, **131**, 7220.
4. A. Dass, P. R. Nimmala, V. R. Jupally and N. Kothalawala, *Nanoscale*, 2013, **5**, 12082.
5. L. J. Cheng, C. D. Ren, X. Z. Zhang and J. L. Yang, *Nanoscale*, 2013, **5**, 1475.
6. M. Z. Zhu, C. M. Aikens, F. J. Hollander, G. C. Schatz and R. C. Jin, *J. Am. Chem. Soc.*, 2008, **130**, 5883.
7. M. W. Heaven, A. Dass, P. S. White, K. M. Holt and R. W. Murray, *J. Am. Chem. Soc.*, 2008, **130**, 3754.
8. H. F. Qian, W. T. Eckenhoff, Y. Zhu, T. Pintauer and R. C. Jin, *J. Am. Chem. Soc.*, 2010, **132**, 8280.
9. C. J. Zeng, H. F. Qian, T. Li, G. Li, N. L. Rosi, B. Yoon, R. N. Barnett, R. L. Whetten, U. Landman and R. C. Jin, *Angew. Chem.*, 2012, **124**, 13291.

10. A. Das, C. Liu, C. J. Zeng, G. Li, T. Li, N. L. Rosi and R. C. Jin, *J. Phys. Chem. A*, 2014, **118**, 8264.
11. P. R. Nimmala, S. Knoppe, V. R. Jupally, J. H. Delcamp, C. M. Aikens and A. Dass, *J. Phys. Chem. B*, 2014, **118**, 14157.
12. C. J. Zeng, T. Li, A. Das, N. L. Rosi and R. C. Jin, *J. Am. Chem. Soc.*, 2013, **135**, 10011.
13. A. Das, T. Li, K. Nobusada, C. Zeng, N. L. Rosi and R. C. Jin, *J. Am. Chem. Soc.*, 2013, **135**, 18264.
14. A. Das, T. Li, G. Li, K. Nobusada, C. J. Zeng, N. L. Rosi and R. C. Jin, *Nanoscale*, 2014, **6**, 6458.
15. S. Chen, S. X. Wang, J. Zhong, Y. B. Song, J. Zhang, H. T. Sheng, Y. Pei and M. Z. Zhu, *Angew. Chem. Int. Ed.*, 2015, **54**, 3145.
16. A. Das, C. Liu, H. Y. Byun, K. Nobusada, S. Zhao, N. Rosi and R. C. Jin, *Angew. Chem.*, 2015, **127**, 3183.
17. A. Dass, S. Theivendran, P. R. Nimmala, C. Kumara, V. R. Jupally, A. Fortunelli, L. Sementa, G. Barcaro, X. Zuo and B. C. Noll, *J. Am. Chem. Soc.*, 2015, **137**, 4610.
18. C. J. Zeng, Y. X. Chen, K. Kirschbaum, K. Appavoo, M. Y. Sfeir and R. C. Jin, *Sci. Adv.*, 2015, **1**, e1500045.
19. Y. X. Chen, C. J. Zeng, C. Liu, K. Kirschbaum, C. Gayathri, R. R. Gil, N. L. Rosi and R. C. Jin, *J. Am. Chem. Soc.*, 2015, DOI: 10.1021/jacs.1025b05378.
20. Y. Negishi, K. Nobusada and T. Tsukuda, *J. Am. Chem. Soc.*, 2005, **127**, 5261.
21. J. Akola, M. Walter, R. L. Whetten, H. Häkkinen and H. Grönbeck, *J. Am. Chem. Soc.*, 2008, **130**, 3756.
22. T. Iwasa and K. Nobusada, *J. Phys. Chem. C*, 2007, **111**, 45.
23. H. Häkkinen, M. Walter and H. Grönbeck, *J. Phys. Chem. B*, 2006, **110**, 9927.
24. N. K. Chaki, Y. Negishi, H. Tsunoyama, Y. Shichibu and T. Tsukuda, *J. Am. Chem. Soc.*, 2008, **130**, 8608.
25. D. E. Jiang, M. L. Tiago, W. D. Luo and S. Dai, *J. Am. Chem. Soc.*, 2008, **130**, 2777.
26. D. E. Jiang, W. D. Luo, M. L. Tiago and S. Dai, *J. Phys. Chem. C*, 2008, **112**, 13905.
27. Y. Pei, Y. Gao and X. C. Zeng, *J. Am. Chem. Soc.*, 2008, **130**, 7830.
28. O. Lopez Acevedo, H. Tsunoyama, T. Tsukuda and C. M. Aikens, *J. Am. Chem. Soc.*, 2010, **132**, 8210.
29. A. Tlahuice-Flores, U. Santiago, D. Bahena, E. Vinogradova, C. V. Conroy, T. Ahuja, S. B. Bach, A. Ponce, G. Wang and M. José Yacamán, *J. Phys. Chem. A*, 2013, **117**, 10470.
30. D. Crasto and A. Dass, *J. Phys. Chem. C*, 2013, **117**, 22094.
31. D. Crasto, S. Malola, G. Brosofsky, A. Dass and H. Häkkinen, *J. Am. Chem. Soc.*, 2014, **136**, 5000.
32. H. Y. Yang, Y. Wang, A. J. Edwards, J. Z. Yan and N. F. Zheng, *Chem. Commun.*, 2014, **50**, 14325.
33. J. Nishigaki, R. Tsunoyama, H. Tsunoyama, N. Ichikuni, S. Yamazoe, Y. Negishi, M. Ito, T. Matsuo, K. Tamao and T. Tsukuda, *J. Am. Chem. Soc.*, 2012, **134**, 14295.
34. Q. M. Wang, Y. A. Lee, O. Crespo, J. Deaton, C. Tang, H. J. Gysling, M. Concepcion Gimeno, C. Larraz, M. D. Villacampa and A. Laguna, *J. Am. Chem. Soc.*, 2004, **126**, 9488.
35. D. E. Jiang, M. Walter and S. Dai, *Chem.Eur. J.*, 2010, **16**, 4999.
36. Y. Pei, N. Shao, H. Li, D. E. Jiang and X. C. Zeng, *ACS nano*, 2011, **5**, 1441.
37. Y. Q. Feng and L. J. Cheng, *RSC Adv.*, 2015, **5**, 62543.
38. D. E. Jiang, W. Chen, R. L. Whetten and Z. F. Chen, *J. Phys. Chem. C*, 2009, **113**, 16983.
39. D. E. Jiang, M. Walter and J. Akola, *J. Phys. Chem. C*, 2010, **114**, 15883.
40. Y. Gao, N. Shao and X. C. Zeng, *ACS nano*, 2008, **2**, 1497.
41. L. J. Cheng, Y. Yuan, X. Z. Zhang and J. L. Yang, *Angew. Chem. Int. Ed.*, 2013, **52**, 9035.
42. P. Maksymovych, D. C. Sorescu and J. T. Yates Jr, *Phys. Rev. Lett.*, 2006, **97**, 146103.
43. S. Knoppe, S. Malola, L. Lehtovaara, T. Bürgi and H. Häkkinen, *J. Phys. Chem. A*, 2013, **117**, 10526.
44. A. Tlahuice-Flores and I. L. Garzón, *Phys. Chem. Chem. Phys.*, 2012, **14**, 7321.
45. A. Tlahuice-Flores, M. Jose-Yacamán and R. L. Whetten, *Phys. Chem. Chem. Phys.*, 2013, **15**, 19557.
46. C. J. Zeng, C. Liu, Y. X. Chen, N. L. Rosi and R. C. Jin, *J. Am. Chem. Soc.*, 2014, **136**, 11922.
47. Y. Pei, J. Tang, X. Q. Tang, Y. Q. Huang and X. C. Zeng, *J. Phys. Chem. Lett.*, 2015, **6**, 1390.
48. A. Genest, S. Krüger, A. B. Gordienko and N. Rösch, *Z. Naturforsch. B*, 2004, **59**, 1585.
49. O. Lopez Acevedo, J. Akola, R. L. Whetten, H. Gronbeck and H. Häkkinen, *J. Phys. Chem. C*, 2009, **113**, 5035.
50. S. Knoppe, O. A. Wong, S. Malola, H. Häkkinen, T. Bürgi, T. Verbiest and C. J. Ackerson, *J. Am. Chem. Soc.*, 2014, **136**, 4129.
51. W. W. Xu, Y. Gao and X. C. Zeng, *Sci. Adv.*, 2015, **1**, e1400211.
52. C. Liu, T. Li, G. Li, K. Nobusada, C. J. Zeng, G. Pang, N. L. Rosi and R. C. Jin, *Angew. Chem. Int. Ed.*, 2015, **54**, 9826.
53. J. Tao, J. P. Perdew, V. N. Staroverov and G. E. Scuseria, *Phys. Rev. Lett.*, 2003, **91**, 146401.
54. A. Lechtken, C. Neiss, M. M. Kappes and D. Schooss, *Phys. Chem. Chem. Phys.*, 2009, **11**, 4344.
55. M. P. Johansson, A. Lechtken, D. Schooss, M. M. Kappes and F. Furche, *Phys. Rev. A*, 2008, **77**, 053202.
56. S. A. Ivanov, I. Arachchige and C. M. Aikens, *J. Phys. Chem. A*, 2011, **115**, 8017.
57. E. D. Glendening, J. K. Badenhoop, A. E. Reed, J. E. Carpenter, J. A. Bohmann, C. M. Morales and F. Weinhold, *Theoretical Chemistry Institute, University of Wisconsin: Madison, WI, 2001*, 2001.
58. M. J. Frisch, H. B. Schlegel, G. E. Scuseria, M. A. Robb, J. R. Cheeseman, G. Scalmani, V. Barone, B. Mennucci, G. A. Petersson, H. Nakatsuji, M. Caricato, X. Li, H. P. Hratchian, A. F. Izmaylov, J. Bloino, G. Zheng, J. L. Sonnenberg, M. Hada, M. Ehara, K. Toyota, R. Fukuda, J. Hasegawa, M. Ishida, T. Nakajima, Y. Honda, O. Kitao, H. Nakai, T. Vreven, J. A. Montgomery, J. E. P. Jr., F. Ogliaro, M. Bearpark, J. J. Heyd, E. Brothers, K. N. Kudin, V. N. Staroverov, T. Keith, R. Kobayashi, J. Normand, K. Raghavachari, A. Rendell, J. C. Burant, S. S. Iyengar, J. Tomasi, M. Cossi, N. Rega, J. M. Millam, M. Klene, J. E. Knox, J. B. Cross, V. Bakken, C. Adamo, J. Jaramillo, R. Gomperts, R. E. Stratmann, O. Yazyev, A. J. Austin, R. Cammi, C. Pomelli, J. W. Ochterski, R. L. Martin, K. Morokuma, V. G. Zakrzewski, G. A. Voth, P. Salvador, J. J. Dannenberg, S. Dapprich, A. D. Daniels, O. Farkas, J. B. Foresman, J. V. Ortiz, J. Cioslowski and D. J. Fox, *Gaussian 09, revision B. 01*, Gaussian, Inc., Wallingford, CT, 2009.
59. U. Varetto, *Swiss National Supercomputing Centre: Manno, Switzerland*, 2009.
60. D. Y. Zubarev and A. I. Boldyrev, *Phys. Chem. Chem. Phys.*, 2008, **10**, 5207.
61. P. J. Hay and W. R. Wadt, *J. Chem. Phys.*, 1985, **82**, 299.
62. A. P. Sergeeva, B. B. Averkiev, H. J. Zhai, A. I. Boldyrev and L. S. Wang, *J. Chem. Phys.*, 2011, **134**, 224304.

63. W. Huang, A. P. Sergeeva, H. J. Zhai, B. B. Averkiev, L. S. Wang and A. I. Boldyrev, *Nat. Chem.*, 2010, **2**, 202.
64. L. J. Cheng, X. Z. Zhang, B. K. Jin and J. L. Yang, *Nanoscale*, 2014, **6**, 12440.
65. D. Y. Zubarev and A. I. Boldyrev, *J. Phys. Chem. A*, 2008, **113**, 866.
66. Y. Pei, S. S. Lin, J. C. Su and C. Y. Liu, *J. Am. Chem. Soc.*, 2013, **135**, 19060.
67. Z. F. Chen and R. B. King, *Chem. Rev.*, 2005, **105**, 3613.
68. P. v. R. Schleyer, C. Maerker, A. Dransfeld, H. J. Jiao and N. J. v. E. Hommes, *J. Am. Chem. Soc.*, 1996, **118**, 6317.
69. A. I. Boldyrev and L. S. Wang, *Chem. Rev.*, 2005, **105**, 3716.
70. J. R. Cheeseman, G. W. Trucks, T. A. Keith and M. J. Frisch, *J. Chem. Phys.*, 1996, **104**, 5497.
71. R. Gershoni Poranne and A. Stanger, *Chem. Soc. Rev.*, 2015, DOI: 10.1039/c1035cs00114e.
72. A. Tlahuice-Flores, R. L. Whetten and M. Jose Yacaman, *J. Phys. Chem. C*, 2013, **117**, 20867.
73. Q. Tang, R. H. Ouyang, Z. Q. Tian and D. E. Jiang, *Nanoscale*, 2015, **7**, 2225.
74. J. Z. Lin, W. L. Li, C. Liu, P. Huang, M. Z. Zhu, Q. J. Ge and G. Li, *Nanoscale*, 2015, **7**, 13663.
75. Y. Yuan, L. J. Cheng and J. L. Yang, *J. Phys. Chem. C*, 2013, **117**, 13276.
76. Y. B. Song, S. X. Wang, J. Zhang, X. Kang, S. Chen, P. Li, H. T. Sheng and M. Z. Zhu, *J. Am. Chem. Soc.*, 2014, **136**, 2963.
77. D. M. Chevrier, A. Chatt, P. Zhang, C. J. Zeng and R. C. Jin, *J. Phys. Chem. Lett.*, 2013, **4**, 3186.
78. X. Li, A. E. Kuznetsov, H. F. Zhang, A. I. Boldyrev and L. S. Wang, *Science*, 2001, **291**, 859.
79. J. O. C. Jiménez Halla, E. Matito, J. Robles and M. Solà, *J. Organomet. Chem.*, 2006, **691**, 4359.
80. M. J. Dewar, *J. Am. Chem. Soc.*, 1984, **106**, 669.
81. K. Exner and P. v. R. Schleyer, *J. Phys. Chem. A*, 2001, **105**, 3407.
82. A. Stanger, *J. Org. Chem.*, 2006, **71**, 883.

